SIAM J. APPL. MATH.
Vol. 70, No. 8, pp. 3022–3038

COMPARISON STUDY OF DYNAMICS IN ONE-SIDED AND TWO-SIDED SOLID-COMBUSTION MODELS*

Y. YANG†, L. K. GROSS‡, AND J. YU†

Abstract. Comparing two-sided and one-sided solid-combustion models, this paper concerns nonlinear transition behavior of small disturbances of front propagation and temperature as they evolve in time. Features include linear instability of basic solutions and weakly nonlinear evolution of small perturbations, as well as the complex dynamics of period doubling, quadrupling, and eventual chaotic oscillations. Both asymptotic and numerical methods are used for different solution regimes. First, multiscale weakly nonlinear analysis takes into account the cumulative effect of small nonlinearities to obtain a correct description of the evolution over long times. For a range of parameters, the asymptotic method with some dominant modes captures the formation of coherent structures. In other cases, numerical solutions reveal period-folding behaviors. In general, the one- and two-sided models agree qualitatively for all solution regimes, which is consistent with prior numerical comparisons and extends our results from [L. K. Gross and J. Yu, *SIAM J. Appl. Math.*, 65 (2005), pp. 1708–1725].

Key words. free-interface problems, free-boundary problems, condensed-phase combustion, marginal instability, weakly nonlinear analysis, asymptotic expansions, Crank–Nicholson method, Fourier transforms

AMS subject classifications. 35R35, 80A25, 80M35, 80M25, 42A38

DOI. 10.1137/090771855

1. Introduction.

In this article we compare quantitatively a weakly nonlinear analysis of a free-interface model of solid combustion with numerical simulations. We also directly compare the dynamics to those in the free-boundary ("one-sided") model we studied in [10].

For the asymptotic method on the free-interface model, we fix the bifurcation parameter ν related to the activation energy to within a rather small number ϵ^2 of the neutrally stable value ν_c, as we did in [10] for the free-boundary model. Within a sufficiently small neighborhood of the neutral stability boundary, Fourier spectra of the numerical quasi–steady-state solutions indicate the dominance of a single mode. We show how the asymptotic solutions capture essential features of the numerical solutions in such regimes.

The spectra also illustrate how period doubling and eventual chaos develop, as a parameter σ related to the Arrhenius kinetics decreases. By varying ϵ, we quantify the domain of applicability of the weakly nonlinear analysis of the free-interface model. In comparing these results with our results [10] on the free-boundary model, we show that the two models produce similar complex dynamics. However, to see the period-doubling cascade in σ in the two-sided model, the bifurcation parameter ν must deviate by a somewhat larger amount ϵ^2 from its critical value than is required in the case of the free-boundary model.

*Received by the editors September 22, 2009; accepted for publication (in revised form) June 30, 2010; published electronically October 21, 2010.
http://www.siam.org/journals/siap/70-8/77185.html
†Department of Mathematics and Statistics, The University of Vermont, Burlington, VT 05405 (yiyang@cems.uvm.edu, jun@cems.uvm.edu).
‡Department of Mathematics and Computer Science, Bridgewater State University, Bridgewater, MA 02325 (laura.gross@bridgew.edu).

The solid-combustion application under consideration refers to a chemical reaction that converts a solid fuel directly into solid products with no intermediate gas phase formation. For example, in self-propagating high-temperature synthesis (SHS), a flame wave advances through powdered ingredients, leaving high-quality ceramic materials or metallic alloys in its wake. (See, for instance, [13, 15, 18].)

The propagation results from the interaction between heat generation and heat diffusion in the material. In some parametric regimes, a balance exists between the two, producing a constant burning rate. In other cases, the interplay between reaction and diffusion results in a wide variety of nonuniform behaviors, including chaos.

In [16], Shkadinsky, Khaikin, and Merzhanov predict the simplest oscillations by numerically solving reaction-diffusion partial differential equations. The system contains Arrhenius-kinetics terms that account for chemical conversion throughout the entire spatial domain.

The literature contains models that employ a variety of approximations to the Arrhenius kinetics. For instance, computations involving Arrhenius kinetics with a cut-off reveal a number of period-doubling bifurcations leading to chaotic pulsations [1].

Other approximations include δ-function kinetics to capture the narrowness of the reaction zone. A point-source model has an exact traveling-wave solution and allows more ready analysis than one with distributed Arrhenius kinetics. In [12], Matkowsky and Sivashinsky study a concentrated-kinetics model in the case of large activation energy and perform an analysis similar to [17].

Numerical solution of this free-interface problem in [4] shows transitions to chaos via a period-doubling solution and highly irregular relaxational oscillations for a sufficiently large activation energy. The authors attribute a lack of sequential secondary bifurcations to discrepancies between the point-source and distributed-kinetics models like those in [1]. Subsequent computations [7], however, show period quadrupling, octupling, etc., for the free-interface model, just as for distributed kinetics.

In [7], the authors also perform numerical computations on a free-boundary model of solid combustion. They motivate it by noting that both the reaction-diffusion model as in [16] and the free-interface model in [12] assume a constant value of thermal diffusivity. However, some problems manifest a clear dependence of this parameter on degree of conversion. In fact, when the burnt product is a foam-like substance, heat diffusion in the product region is negligible. For such cases, they consider a model that includes the heat equation on a semi-infinite domain ahead of the reaction and a nonlinear kinetic condition imposed on the moving boundary. In [10] we quantitatively compare a weakly nonlinear analysis of the free-boundary model with numerical simulations.

Note that both the free-interface (two-sided) model and the free-boundary (one-sided) model stem from reaction-diffusion partial differential equations with full Arrhenius kinetics. To emphasize, the one-sided model is not an adaptation of the two-sided model; rather, each of them is a viable derivative of the reaction-diffusion model. The two-sided model assumes a single constant conductivity throughout the reactant and product zones. The one-sided model assumes zero conductivity in the burned region. In some cases the first approximation is more appropriate and in others the second is.

The models discussed in this literature review all produce the same nonlinear dynamics as experiments. Belyaev and Komkova discovered pulsations in the burning of a chrome-magnesium thermite in 1950 [2]. A planar front may have oscillated with

a constant frequency in their experiments, but they did not observe the process in detail. Later Merzhanov, Filonenko, and Borovinskaya [14] observed experimentally both the periodic propagation of a flat front in SHS, as well as spinning waves, showing a fuller understanding of the behaviors. The dynamical scenarios agree with computed solutions of (i) the reaction-diffusion system governed by the full Arrhenius kinetics (e.g., [5]), (ii) the reaction-diffusion system with Arrhenius kinetics with a cut-off (e.g., [1]), and models that use point-source kinetics like (iii) the free-interface ("two-sided") model with constant heat diffusivity (e.g., [7]), as well as (iv) the free-boundary ("one-sided") model, in which heat transfer behind the flame front (in the burned matter) is qualitatively unimportant (e.g., [6]). However, the stability thresholds for uniformly propagating fronts differ for the different kinetics mentioned, and one has only approximate numerical values for distributed kinetics.

Simulations on all these models show the same dynamics, as one pushes the bifurcation parameter deeper into the instability regions. In particular, numerical simulations and analysis in [7] show that such dynamics of the two-sided and one-sided problems agree extremely closely. By contrast, in the present work, we retain the bifurcation parameter ν within ϵ^2 of the neutrally stable value and vary the kinetics parameter σ, rather than exploring regimes more and more strongly unstable in ν. In addition, we vary ϵ, thereby also changing ν, and study the impact on the dynamics with respect to the kinetics parameter σ. We then compare results from the two- and one-sided models.

Two-dimensional combustion can be described by a one-dimensional model when the only unstable mode corresponds to the dynamics with no spatial variation in the transverse direction. For example, the linear stability analysis in [9] shows that for a free-boundary model, a flat front dominates the behavior for the case of a sufficiently narrow strip of material with insulated edges.

Dynamics of point-source models have also been studied with perturbation techniques. In [11, 8], intricate bifurcation analyses classify the interactions of clockwise and counterclockwise spinning waves on the surface of a cylinder. Margolis's review paper [11] includes a thorough discussion of resonance phenomena, treating sample radii that yield close, as well as equal, eigenvalues. Also, Booty, Margolis, and Matkowsky [3] predict cascades of bifurcations from a double eigenvalue of a linearized model of condensed-phase combustion in a long cylindrical sample. They show that the inclusion of melting in the model makes the neutral-stability threshold more accessible. A bifurcation parameter ν in the present work is restricted to a smaller neighborhood of the value corresponding to a single neutrally stable eigenvalue. In studying the nonlinear transition behavior of small disturbances of front propagation and temperature as they evolve in time, we compare quantitatively (section 3) the results of weakly nonlinear analysis (section 2) with direct simulations. In section 4, we compare results from the free-interface model of section 2 with our results on the free-boundary model [10].

2. Mathematical analysis. To start, we use the sharp-interface model of solid combustion introduced by Matkowsky and Sivashinsky [12]. It includes the heat equation posed ahead of and behind a free boundary, as well as a nonlinear kinetic condition imposed at the interface. Because of the semi-infinite domain on each side of the front, this model is referred to as a two-sided model.

To solve, we seek the temperature distribution $u(x,t)$ in one spatial dimension and the interface position $\Gamma(t) = \{x \mid x = f(t)\}$ that satisfy the appropriately non-

dimensionalized free-boundary problem

$$\frac{\partial u}{\partial t} = \frac{\partial^2 u}{\partial x^2}, \quad x \neq f(t), \quad t > 0, \tag{2.1}$$

$$V = G\left(u\big|_{\Gamma}\right), \quad t > 0, \tag{2.2}$$

$$\left.\frac{\partial u}{\partial x}\right|_{\Gamma^+} - \left.\frac{\partial u}{\partial x}\right|_{\Gamma^-} = -V, \quad t > 0. \tag{2.3}$$

Here V is the velocity of the rightward-traveling interface, i.e., $V = df/dt$. In addition, the temperature satisfies the condition $u \to 0$ as $x \to \infty$; that is, the ambient temperature is normalized to zero at infinity. We also require the temperature $u(x,t)$ to remain bounded as $x \to -\infty$ (behind the front).

To model solid combustion, we take the Arrhenius function as the kinetics function G in the nonequilibrium interface condition (2.2) [4, 15]. Then, with appropriate nondimensionalization, the velocity of propagation relates to the interface temperature as

$$V = \exp\left[\left(\frac{1}{\nu}\right)\frac{u-1}{\sigma + (1-\sigma)u}\right] \tag{2.4}$$

at the interface Γ. In terms of dimensional parameters, the dimensionless parameters are $\nu = \frac{RT_b^2}{(T_b - T_0)E}$ and $0 < \sigma = \frac{T_0}{T_b} < 1$, following [4], where T_0 is the ambient temperature, T_b is the adiabatic temperature of combustion products, R is the universal gas constant, and E is the activation energy of the exothermic chemical reaction that occurs at the interface.

A front-attached coordinate frame

$$\eta = x - f(t), \quad \tau = t$$

proves convenient for asymptotic and numerical analysis. After this change of variables, the problem admits a traveling-wave solution

$$u_0(\eta,\tau) = g_0(\eta) = \begin{cases} e^{-\eta} & \text{if } \eta \geq 0, \\ 1 & \text{if } \eta < 0, \end{cases} \qquad f_0(\tau) = \tau. \tag{2.5}$$

The problem linearized about the traveling wave has a normal-mode solution of the form

$$w = e^{\lambda\tau} g(\eta;\lambda), \quad \phi = e^{\lambda\tau},$$

where w and ϕ represent the perturbations about u_0 and f_0, respectively. Substituting them into the linearized problem produces an eigenvalue problem in λ and $g(\eta;\lambda)$.

The discrete spectrum values are zero and

$$\lambda = \frac{-\left(\nu^2 + 4\nu - 1\right) \pm \sqrt{\left(\nu^2 + 4\nu - 1\right)^2 - 16\nu^3}}{8\nu^2}.$$

The eigenfunction corresponding to the eigenvalue λ is

$$g(\eta;\lambda) = \begin{cases} \frac{\nu + \nu\sqrt{1+4\lambda} - 2}{2\nu\sqrt{1+4\lambda} - 2} \exp\left(-\left(1 + \sqrt{1+4\lambda}\right)\frac{\eta}{2}\right) - e^{-\eta} & \text{if } \eta \geq 0, \\ \frac{\nu - \nu\sqrt{1+4\lambda}}{2\nu\sqrt{1+4\lambda} - 2} \exp\left(-\left(1 - \sqrt{1+4\lambda}\right)\frac{\eta}{2}\right) & \text{if } \eta < 0. \end{cases}$$

The basic solution (2.5) is neutrally stable under a small perturbation if $\Re\lambda = 0$. Setting $\Re\lambda = 0$ gives the critical value ν_c of ν, namely,

$$\nu_c = \sqrt{5} - 2. \tag{2.6}$$

(See also [12].) The corresponding neutrally stable eigenvalues are $\pm i\omega$, where

$$\omega = \frac{\sqrt{\sqrt{5}+2}}{2}. \tag{2.7}$$

If $\nu < \sqrt{5} - 2$, then $\Re\lambda > 0$, and the basic solution is linearly unstable.

For the weakly nonlinear analysis, let ϵ^2 be a small deviation from the neutrally stable value of ν, namely,

$$\epsilon^2 = \nu_c - \nu = \sqrt{5} - 2 - \nu. \tag{2.8}$$

We consider the time scales

$$t_0 = \tau, \quad t_1 = \epsilon\tau, \quad t_2 = \epsilon^2\tau$$

as independent variables, so that $\partial/\partial\tau = \partial/\partial t_0 + \epsilon\,\partial/\partial t_1 + \epsilon^2\,\partial/\partial t_2$.

We perturb the basic solution (2.5) by ϵ times the most linearly unstable mode, evaluated at both the neutrally stable parameter value $\nu = \nu_c$ and the corresponding neutrally stable eigenvalue. The normal-mode perturbations are modulated by complex-valued, slowly varying amplitude functions. In particular, we seek a solution of the form $u = u(\eta, t_0, t_1, t_2)$, $f = f(t_0, t_1, t_2)$,

$$u = g_0(\eta) + \epsilon A(t_1, t_2)\, e^{i\omega t_0} g(\eta; i\omega, \nu_c) + \epsilon^2 w_2(\eta, t_0, t_1, t_2) + \cdots + CC, \tag{2.9}$$

$$f = t_0 + \epsilon\left\{A(t_1, t_2)\, e^{i\omega t_0} + \frac{1}{2}B(t_1, t_2)\right\} + \epsilon^2\phi_2(t_0, t_1, t_2) + \cdots + CC, \tag{2.10}$$

where $A(t_1, t_2)$ is complex, and "CC" stands for complex-conjugate terms. The real-valued function $B(t_1, t_2)$ modulates the constant-velocity solution to the linearized problem.

Notice that in $O(\epsilon)$, the weakly nonlinear solution (2.9)–(2.10) has only one Fourier term in t_0. The $O(\epsilon^2)$ terms contain the second harmonic. We refer to the expansion above as a single-mode approximation because the leading-order perturbation contains only one mode in fast time.

Using the above expansion and equating like powers of ϵ results in subproblems for the terms in the perturbation expansions above, subject to solvability conditions on the amplitudes A and B. In particular, according to Fredholm's alternative, each subproblem has a nonsecular (bounded in time) solution if the right-hand side is orthogonal to the null space of the adjoint operator $\mathcal{L}^*$.

This weakly nonlinear analysis leads to

$$\frac{\partial A}{\partial t_1} = 0,$$

$$\frac{\partial B}{\partial t_1} = A\bar{A}r_0,$$

$$\frac{dA}{dt_2} = \chi A + \beta A^2\bar{A}, \tag{2.11}$$

where r_0, χ, and β are complex constants. See the appendix for details. (See also [10] for the one-sided-model analogue we discuss in section 4.)

The evolution equation (2.11) has circular limit cycles in the complex-A plane for all values of the kinetic parameter σ in the interval $0 < \sigma < 1$ (i.e., for all physical values of σ). To find $A(t_2)$, we integrate the ordinary differential equation (2.11) using a fourth-order Runge–Kutta method.

3. Results and discussion for two-sided model. To compare quantitatively the asymptotics with the numerics, we first consider $\epsilon = 0.1$. The value of ν remains at the marginally unstable value $\nu_c - \epsilon^2$, as in (2.8), i.e., $\sqrt{5} - 2.01$. We show in this section that for this choice of ϵ the dynamics qualitatively do not vary much as σ varies. Note that for ν to remain fixed as σ decreases, the (dimensional) activation energy E could be decreased appropriately. Subsequently, we will comment on the impact on the front behavior of both decreasing and increasing ϵ (and thereby $\nu = \nu_c - \epsilon^2$).

To start, take $\sigma = 0.48$ in the kinetics function (2.4). For the remainder of this paper we take the initial condition $A(0) = 0.1$.

Figure 1 shows the numerical (solid line) and asymptotic (dashed line) values of front speed perturbation as a function of time t in the interval $0 \le t \le 100$. The asymptotic solution in the figure (dashed line) is the perturbation to the traveling-wave solution (divided by ϵ) described in the previous section. In calculating the asymptotic solution, we integrate the ordinary differential equation (2.11) using a fourth-order Runge–Kutta method. To obtain the numerical solution (solid line in Figure 1), we used the Crank–Nicholson method to solve the problem in a front-attached coordinate frame. The method is analogous to that used in [10] for the one-sided model we describe in section 4.

Figure 1 reveals that from $t = 0$ to about $t = 40$, the small front speed perturbation is linearly unstable, and its amplitude grows exponentially in time. As this amplitude becomes large, nonlinearity takes effect. At around $t = 40$, the front speed perturbation has reached steady oscillation. The two solutions are slightly out

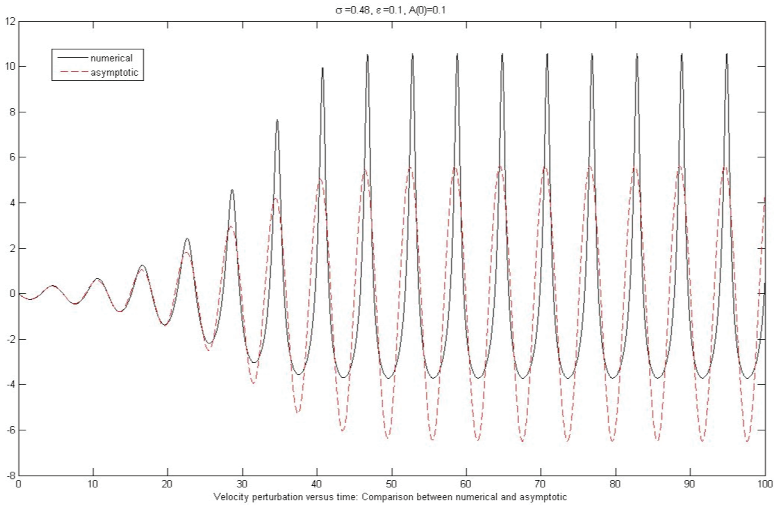

FIG. 1. *Velocity perturbation versus time: Comparison between numerical (solid line) and asymptotic (dashed line) for Arrhenius kinetics;* $\sigma = 0.48$, $\epsilon = 0.1$, $A(0) = 0.1$ *(*$\nu \approx \nu_c - \epsilon^2 = \sqrt{5} - 2 - (0.1)^2 \approx 0.226067977$*).*

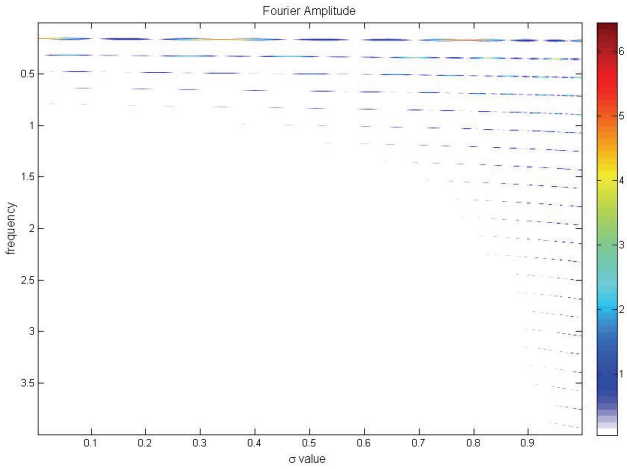

FIG. 2. *Amplitudes corresponding to each frequency of the Fourier transformed velocity perturbation data for the Arrhenius kinetics parameter* σ *in the interval* $(0, 1)$, $\epsilon = 0.1$, $A(0) = 0.1$, $1000 < t < 1500$ *(*$\nu \approx \nu_c - \epsilon^2 = \sqrt{5} - 2 - (0.1)^2 \approx 0.226067977$*).*

of phase, and the asymptotic solution oscillates symmetrically about the time axis, while the numerical solution has spiky peaks. The asymptotic solution accurately captures the period in both transient behavior for $t = 0$ to 40 and the long-time behavior after $t = 40$. This is an example in which the weakly nonlinear approach describes rather well the marginally unstable large-time behavior: A single modulated temporal mode captures the period of fluctions in velocity perturbation.

To identify such regimes systematically, we calculate numerically the velocity perturbation data on the time interval $1000 < t < 1500$, throughout the range of physical values of the kinetics parameter σ (i.e., $0 < \sigma < 1$). Figure 2 summarizes the Fourier transformed velocity data for $\epsilon = 0.1$. For each σ value and each frequency, the color indicates the corresponding amplitude, with the red end of the spectrum standing for larger numbers than those the violet end represents. On almost the whole interval $0 < \sigma < 1$, the figure shows the dominance of the lowest-order mode. However, additional frequencies also contribute to the solutions, producing some discrepancies with the asymptotic solution visible in Figure 1. As σ increases, more and more higher-order modes affect the dynamics, producing increasingly sharp spikes in the velocity profiles.

As we increase ϵ to about 0.145, period-replicating cascades emerge for some σ values. To illustrate such regimes, we increase ϵ to 0.l8 and calculate numerically the velocity perturbation data on the time interval $1000 < t < 1500$ throughout the range of physical values of the kinetics parameter σ $(0 < \sigma < 1)$. Figure 3 summarizes the Fourier transformed velocity data. As in Figure 2, we see the dominance of the lowest-order mode on most of the σ interval. However, higher-order modes also contribute. In particular, when σ is greater than approximately 0.60, solutions have sharp peaks (sharper than the numerical solution in Figure 1). A careful look at Figure 3 shows that period doubling occurs when σ is decreased to approximately 0.53. Figure 4 gives a closer view of the dominant modes for smaller σ values; notice the bifurcation to period quadrupling near $\sigma = 0.09$ and period octupling near $\sigma = 0.045$. The cascade of period-doubling solutions for decreasing σ leads to chaos. The four numerical

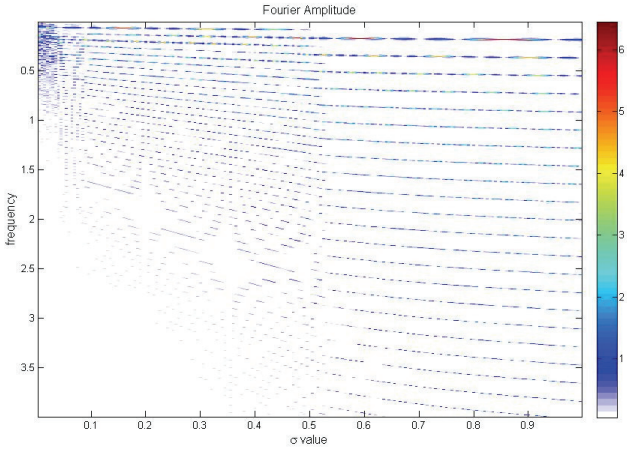

FIG. 3. *Amplitudes corresponding to each frequency of the Fourier transformed velocity perturbation data for the Arrhenius kinetics parameter σ in the interval $(0, 1)$, $\epsilon = 0.18$, $A(0) = 0.1$, $1000 < t < 1500$ ($\nu \approx \nu_c - \epsilon^2 = \sqrt{5} - 2 - (0.18)^2 \approx 0.203667977$).*

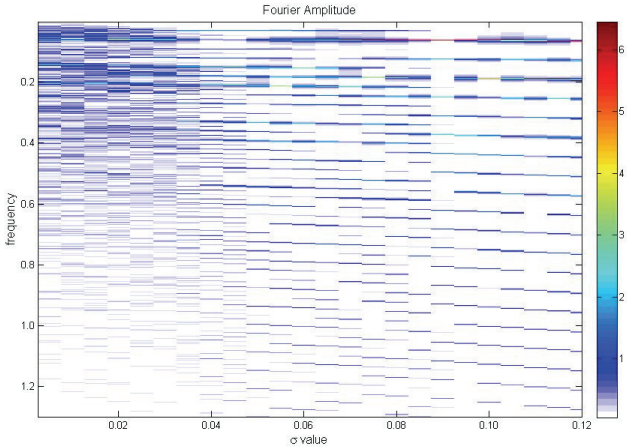

FIG. 4. *Amplitudes corresponding to each frequency of the Fourier transformed velocity perturbation data for the Arrhenius kinetics parameter σ in the interval $(0, 0.12)$, $\epsilon = 0.18$, $A(0) = 0.1$, $1000 < t < 1500$ ($\nu \approx \nu_c - \epsilon^2 = \sqrt{5} - 2 - (0.18)^2 \approx 0.203667977$).*

solutions in Figures 5 and 6 illustrate the cascade of period-replicating solutions, including doubling ($\sigma = 0.48$), quadrupling ($\sigma = 0.058$), and octupling ($\sigma = 0.045$).

As the parameter ν decreases ever further from the neutrally stable value (i.e., as ϵ increases), the σ interval in which one mode dominates strongly shrinks and disappears. By contrast, when ϵ shrinks to 0.145, the period-replicating dynamics—including eventual chaos—disappear. For example, when $\epsilon = 0.1$, the asymptotic and numerical solutions are comparable throughout most of the physical range of σ ($0 < \sigma < 1$). (See Figures 1 and 2.) Varying ϵ quantifies the domain of applicability of the weakly nonlinear analysis and delineates the role of σ in the dynamics.

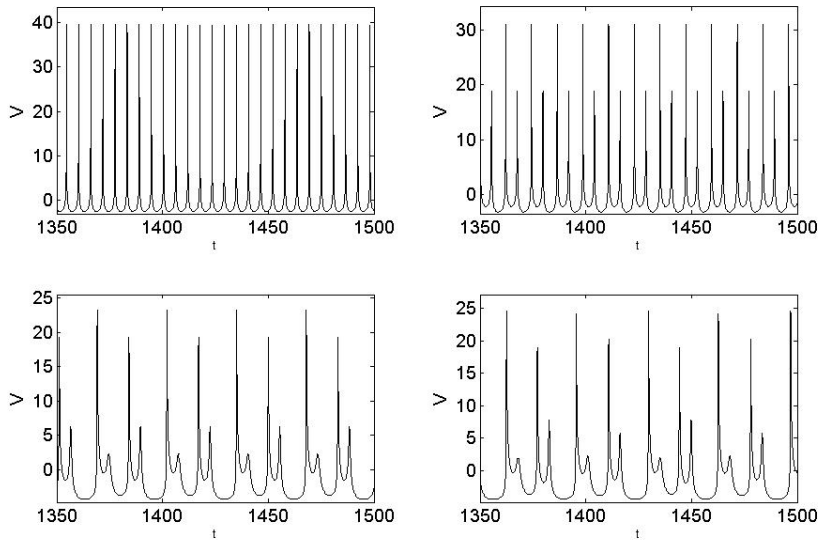

FIG. 5. *Velocity perturbations versus time* ($\epsilon = 0.18$, $A(0) = 0.1$, $\nu = \nu_c - \epsilon^2 \approx \sqrt{5} - 2 - (0.18)^2 \approx 0.203667977$). *Upper left: Quasi-periodic solution for* $\sigma = 0.65$. *Upper right: Period doubling* ($\sigma = 0.48$). *Lower left: Period quadrupling* ($\sigma = 0.058$). *Lower right: Period octupling* ($\sigma = 0.045$).

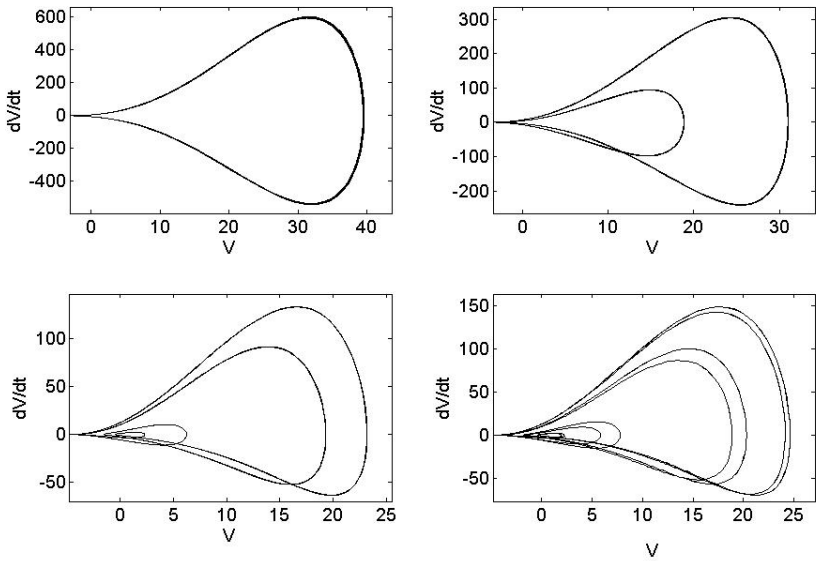

FIG. 6. *Phase plots of the four solutions of Figure* 5 *for* $1350 < t < 1500$: *Velocity perturbations* $v(t)$ *versus* dv/dt.

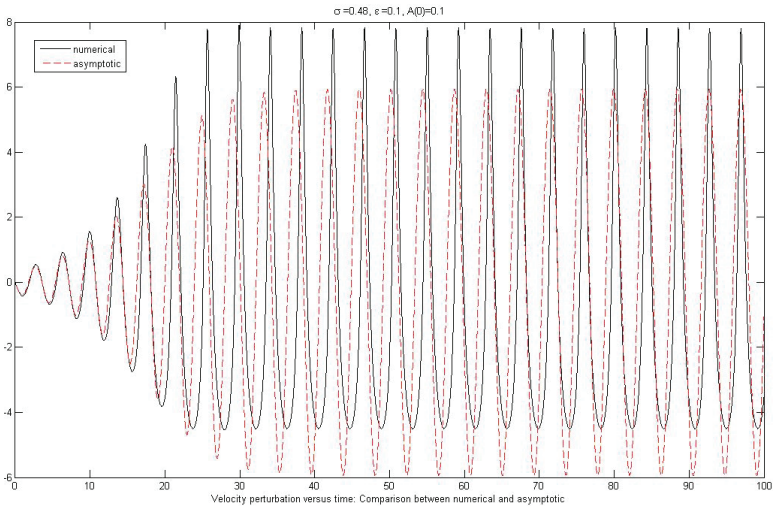

FIG. 7. *Velocity perturbation versus time: Comparison between numerical (solid line) and asymptotic (dashed line) for the one-sided model;* $\sigma = 0.48$, $\epsilon = 0.1$, $A(0) = 0.1$ *(*$\nu \approx \nu_c - \epsilon^2 = 1/3 - (0.1)^2 = 0.32\bar{3}$*). This figure first appeared in* [10].

4. Comparison with the one-sided model. As mentioned earlier, the thermal diffusivity in the reaction-diffusion model could depend on the degree of conversion, and in some cases it is negligible in the product region. For such cases, some authors have analyzed a so-called one-sided model of solid combustion as a viable derivative of the reaction-diffusion model. (See, for example, [7].) They consider a model identical to the model in section 2, except that the domain for the partial differential equation (2.1) is the region ahead of the front only, i.e., $x > f(t)$, rather than the two sides of the front $(-\infty, f(t))$ and $(f(t), \infty)$. The model uses the condition

$$\left.\frac{\partial u}{\partial x}\right|_{\Gamma} = -V, \quad t > 0, \tag{4.1}$$

in place of jump condition (2.3). It omits the condition that $u(x,t)$ remain bounded as $x \to -\infty$, as the problem is posed on the semi-infinite domain to the right of $f(t)$ only.

We compare the results of section 3 with the analogous results [10] on the free-boundary model. Note first that the basic solutions coincide ahead of the front: For the one-sided model we neglect the interval $x < f(t)$ behind the reaction in the traveling-wave solution (2.5). We perturb the basic solution for each model to study the nonlinear dynamics in the marginally unstable regimes, i.e., for an $O(\epsilon^2)$ perturbation around the critical value of ν as in (2.8).

For the two-sided model, $\nu_c = \sqrt{5} - 2$ as in (2.6). For the one-sided model,

$$\nu_c = \frac{1}{3}. \tag{4.2}$$

(See, for example, [10].) Note that allowing the burned region as a heat sink in the two-sided model stabilizes the dynamics; ν must drop to $\sqrt{5} - 2$ before the traveling wave loses stability. In both models the weakly nonlinear dynamics are governed by the Landau–Stuart equation (2.11) with different parameters χ and β. (See, for example, [10] for details in the one-sided case.)

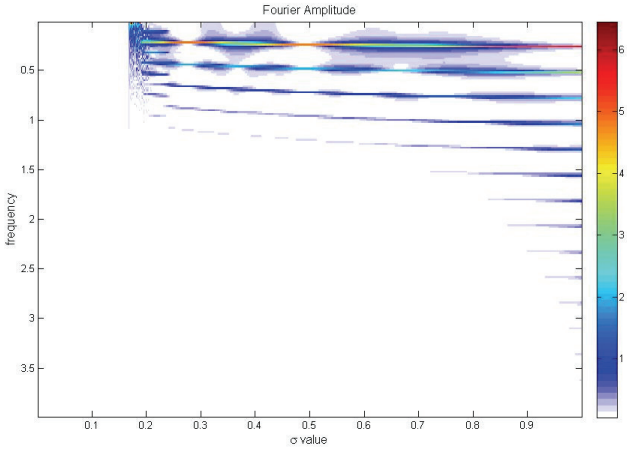

FIG. 8. *Amplitudes corresponding to each frequency of the Fourier transformed velocity perturbation data for the Arrhenius kinetics parameter σ in the interval $(0, 1)$ for the one-sided model; $\epsilon = 0.1$, $A(0) = 0.1$, $35 < t < 85$ ($\nu \approx \nu_c - \epsilon^2 = 1/3 - (0.1)^2 = 0.32\overline{3}$). This figure first appeared in* [10].

The plot of time versus velocity perturbation in Figure 7 (adapted from [10]) for the one-sided model is similar to that in Figure 1 for the two-sided model. For example, the asymptotic solutions for both cases capture the period of the numerical solutions well. However, the two-sided asymptotic velocity profile seems to "undershoot" the corresponding numerical solution more.

For comparison with Figure 2, we calculate numerically the velocity perturbation data for the one-sided model on the time interval $35 < t < 85$ throughout the range of physical values of the kinetics parameter σ (i.e., $0 < \sigma < 1$). Figure 8 (adapted from [10]) summarizes the Fourier transformed velocity data for each σ value and each frequency, with the color indicating the corresponding amplitude as in Figures 2–4. For roughly $0.3 < \sigma < 0.6$, the figure shows the dominance of the lowest-order mode, suggesting the appropriateness of the weakly nonlinear analysis in this range. For other values of σ, a single mode cannot be expected to capture the full dynamics of the solution.

In particular, when σ is greater than 0.6, solutions have sharp peaks—sharper than the numerical solution in Figure 7 for $\sigma = 0.48$. However, we show later that solutions for the two-sided model have even sharper peaks. Figure 8 shows that when σ is smaller than approximately 0.3, the Fourier spectrum has a complicated character, starting with the emergence of a period-doubling solution for $\sigma \approx 0.25$. In contrast, Figure 2, corresponding to the two-sided model, shows no period-replicating cascades as σ decreases to zero. To see such a picture for the one-sided model, ϵ must be reduced from 0.1 to around 0.06. See [10].

Note that Figure 8 reflects the breakdown of the numerical solution for σ less than approximately 0.19. We see such a breakdown for the two-sided case for small σ only when ϵ gets as large as 0.25. Numerical simulation shows that for these cases the interface velocity V drops to near zero and stays there for hundreds of time units. When the interface velocity is very close to zero, the numerical solutions for the temperature distributions $u(\eta, t)$ may strongly depend on the interval length L. The partial derivative $\partial u/\partial \eta$ at $\eta = L$ may be markedly different from zero

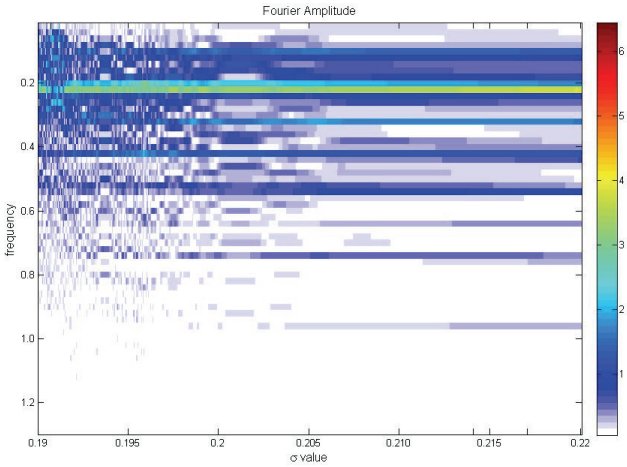

FIG. 9. *Amplitudes corresponding to each frequency of the Fourier transformed velocity perturbation data for the Arrhenius kinetics parameter σ in the interval $(0.19, 0.22)$ for the one-sided model; $\epsilon = 0.1$, $A(0) = 0.1$, $35 < t < 85$ ($\nu \approx \nu_c - \epsilon^2 = 1/3 - (0.1)^2 = 0.32\bar{3}$). This figure is adapted from a figure that first appeared in* [19]. *Our figure appears here with permission from John Wiley and Sons (http://onlinelibrary.wiley.com/journal/*10.1002*/(ISSN)*1099-0526*).*

and will decrease with L more slowly than L^{-1}. Here L is used in the Dirichlet condition $u(L,t) = 0$ to simulate the condition $u \to 0$ when $\eta \to \infty$. For these cases the prevailing arithmetic could not be efficiently used in simulating the decay of the temperature at infinity. Although one could further probe the sensitivity of the interface velocity V to the boundary condition at infinity, at present the authors would like to emphasize the nonlinear dynamics associated with combinations of values for parameters ϵ and σ for which this issue is less relevant. As an example, Figure 3 shows numerical results on the two-sided model for all physical σ values when ϵ equals 0.18.

Figure 9 gives a closer look at the dominant modes for an interval of small σ values; notice the bifurcation to a six-folding solution near $\sigma = 0.201$. The four numerical solutions in Figures 10 and 11 illustrate the cascade of period-replicating solutions, including doubling ($\sigma = 0.22$), quadrupling ($\sigma = 0.21$), and six-folding ($\sigma = 0.2015$). (Figures 9–11 are adapted from figures that first appeared in [19].) The cascade of period-replicating solutions for decreasing σ leads to chaos.

Notice that numerical solutions to the one-sided model (Figures 7, 10, and 11) are less sharply pointed than solutions to the two-sided model (Figures 1, 5, and 6). Multimode components in the two-sided solutions probably explain this difference.

In particular, the nonlinear interface condition (2.2) of the two-sided model couples modes from two regions, yielding more interaction than in the one-sided model. To adequately describe the system with the same parameters requires more dynamical modes for the two-sided model than for the one-sided model. For weakly nonlinear cases in the two-sided model, the interaction between the modes in the two regions is small; evolution on one side is similar to that described by the one-sided model, and so the Landau–Stuart equation (2.11) with appropriate coefficients is applicable. In more general cases of strong nonlinearity, the nonlinear interaction between modes in the two regions is strong, leading to features that differ from solutions to the one-sided model, such as sharper spikes in the velocity profiles as shown in our numerical

results.

From a broader point of view, both the free-interface (two-sided) model and the free-boundary (one-sided) model can be regarded as limiting cases of a more general model that allows for different thermal conductivities in the reactant and product zones. Assuming the conductivities in the unburned and burned regions are 1 and a_p, respectively, the two-sided model (2.1)–(2.4) can be generalized by replacing (2.1) with

$$\frac{\partial u}{\partial t} = \frac{\partial^2 u}{\partial x^2}, \qquad f(t) < x < \infty, \quad t > 0,$$

$$\frac{\partial u}{\partial t} = a_p \frac{\partial^2 u}{\partial x^2}, \qquad -\infty < x < f(t), \quad t > 0,$$

and, consequently, substituting the boundary condition (2.3) with

$$\left.\frac{\partial u}{\partial x}\right|_{\Gamma+} - a_p \left.\frac{\partial u}{\partial x}\right|_{\Gamma-} = -V, \ \ t > 0.$$

It is easy to show that $a_p = 0$ and $a_p = 1$ correspond to the one-sided model and the two-sided model, respectively. Noticing that (2.5) is also a traveling-wave solution to the generalized solid-combustion model, the linear stability analysis of the basic traveling wave leads to the dispersion relation

$$-\nu(2\lambda + 1)\sqrt{1 + 4a_p\lambda} = 2\nu^2(1 - a_p)\lambda^2 + (4\nu - 2)\lambda + \nu.$$

The dispersion relation reduces to the dispersion relation for the one-sided model (equation (1.14) in [10]) when $a_p = 0$ and to the two-sided model (equation (14) in [7]) when $a_p = 1$. We envision a more detailed investigation of the evolution of the nonlinear dynamics as a function of the thermal conductivity in the product zone a_p in a future publication. In this paper we compare the dynamics of the limiting cases of one-sided and two-sided solid-combustion models.

In summary, linear instability provides a mechanism for transition to nonlinear coherent structures. We have done a weakly nonlinear analysis of the evolution of small disturbances during this transition, providing insight into the nonlinear dynamics we have also investigated numerically. In general, the one- and two-sided models agree qualitatively for all solution regimes, which is consistent with prior numerical comparisons on both Arrhenius and so-called p-q kinetics [7].

Appendix. The complex coefficients r_0, χ, and β in the solvability conditions at the end of of section 2 are defined as follows:

$$r_0 = -\omega^2 \left[\frac{4}{\sqrt{1 + 4i\omega} + \sqrt{1 - 4i\omega}} + K \right],$$

where ω is defined in (2.7), and

$$K = -1 + 2\nu_c(1 - \sigma)$$

for ν_c as defined in (2.6);

$$\chi = 2\omega^3 \left[4\omega \left(2\omega^2 - 1 \right) + i \right];$$

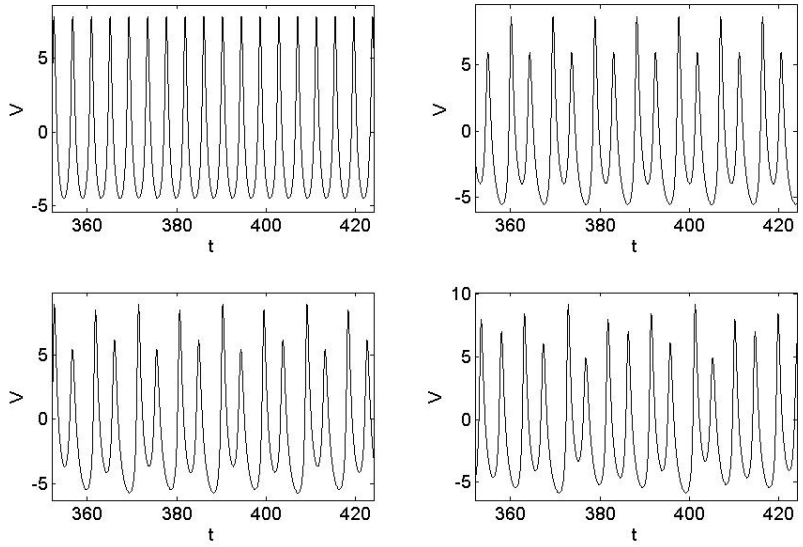

FIG. 10. *Velocity perturbations versus time* ($\epsilon = 0.1$, $A(0) = 0.1$, $\nu \approx \nu_c - \epsilon^2 = 1/3 - (0.1)^2 = 0.32\bar{3}$) *for the one-sided model. Upper left: Quasi-periodic solution for* $\sigma = 0.48$ *(cf. Figure* 7*). Upper right: Period doubling* ($\sigma = 0.22$). *Lower left: Period quadrupling* ($\sigma = 0.21$). *Lower right: Period six-folding* ($\sigma = 0.2015$). *This figure is adapted from a figure that first appeared in* [19]. *Our figure appears here with permission from John Wiley and Sons (http://onlinelibrary.wiley.com/journal/*10.1002*/(ISSN)*1099-0526*).*

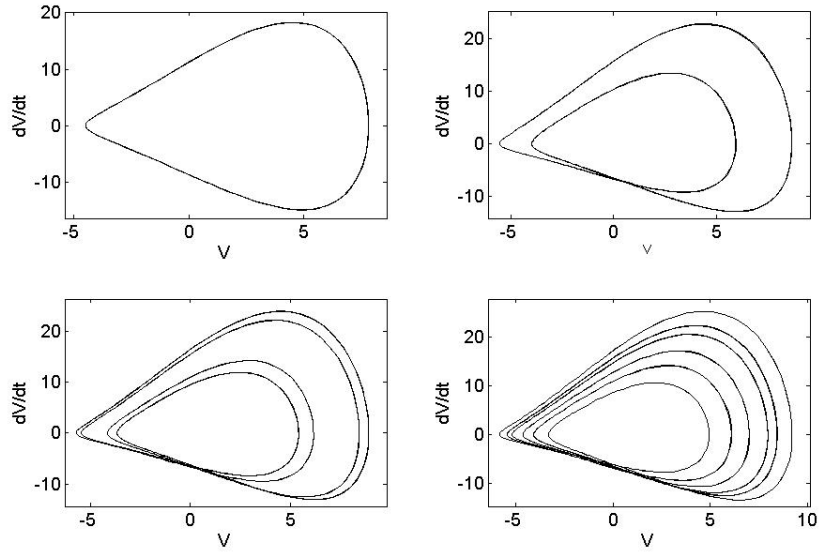

FIG. 11. *Phase plots of the four solutions in Figure* 10 *for the one-sided model: Velocity perturbation* $v(t)$ *versus* dv/dt. *This figure is adapted from a figure that first appeared in* [19]. *Our figure appears here with permission from John Wiley and Sons (http://onlinelibrary.wiley.com/journal/*10.1002*/(ISSN)*1099-0526*).*

and

$$\beta = \frac{\chi_3}{\chi_0}.$$

Here

$$\chi_0 = \frac{(1+\mu_+ - 4\omega^2)i}{\omega\,(1-4\omega i)} - \frac{2\omega + i}{2\omega\sqrt{1+4\omega i}},$$

$$\chi_3 = \frac{\mu_+ - 4\omega^2 + 1}{1-4\omega i} A_{30} + \left(\frac{\mu_+ - 4\omega^2 + 4\omega i}{1-4\omega i} - \overline{\mu_-}\right) E_3 + \left(\frac{\mu_+ - 4\omega^2 + 4\omega i}{1-4\omega i} - \rho_-\right) G_3$$
$$+ \left(\overline{\mu_+} - \mu_+\right) J_3 + (\rho_+ - \mu_+)\, K_3 + I_{30} + \beta_{30} - B_3 - D_{30},$$

where

$$\mu_\pm = \frac{-1 \pm \sqrt{1+4i\omega}}{2}\,, \quad \rho_\pm = \frac{-1 \pm \sqrt{1+8i\omega}}{2},$$

$$A_{30} = \left(O_{20} + \overline{O_{20}}\right)\left(1 - \frac{i}{\omega}\right) - \frac{i}{\omega} B_{10} - 4\omega i\,(K_{20} + L_{20}) + I_{20} - N_{20} - \overline{N_{20}}$$
$$+ K\left[B_{10} - 4\omega^2\,(K_{20} + L_{20}) - \frac{\omega^2}{2} K - \frac{i\omega}{2}\right] + \frac{\omega^2}{2} L,$$

$$E_3 = -2i\omega\overline{\mu_-}\,(K_{20} + L_{20})\,\overline{\Gamma_-} - \frac{i\omega\overline{\mu_-}}{4} K\overline{\Gamma_-} + \frac{\overline{\mu_-}}{2}\overline{M_{20}},$$

$$G_3 = \rho_- J_{20},$$

$$J_3 = -\frac{\overline{\mu_+}}{2}\,(K_{20} + L_{20}) - \frac{\overline{\mu_+}}{16} K + \frac{\overline{\mu_+}}{2}\overline{P_{20}},$$

$$K_3 = \rho_+ L_{20},$$

$$I_{30} = -\frac{\Gamma_+ \mu_+ B_{10} + i\omega\mu_+\,(P_{20} - K_{20})}{2\mu_+ + 1},$$

$$\beta_{30} = -i\omega K\left[4\omega^2\,(K_{20} + L_{20}) + \frac{\omega^2}{2} K\right] + \frac{i\omega^3}{2} L,$$

$$B_3 = -\left(O_{20} + \overline{O_{20}}\right),$$

$$D_{30} = -\frac{\Gamma_- \mu_- B_{10} + i\omega\mu_-\,(M_{20} - H_{20})}{2\mu_- + 1},$$

$$\Gamma_+ = \frac{i}{4\omega}\,, \quad \text{and} \quad \Gamma_- = 1 + \Gamma_+.$$

We list the remaining quantities below in alphabetical order:

$$B_{10} = i\omega\,(\mu_+ - \overline{\mu_+}) - \omega^2 K,$$

$$H_{20} = \mu_- \Gamma_-,$$

$$I_{20} = \frac{\omega\left\{1-\nu_c\sqrt{1+8\omega i}\ \left[1+i\omega K/2\right]\right\}+i\left(\mu_+-\rho_+\right)\left(\mu_+\Gamma_+ +\mu_-\Gamma_-\right)}{2\omega-2\omega\nu_c\sqrt{1+8\omega i}+i\rho_+},$$

$$J_{20} = \frac{\left(\mu_+-\rho_+\right)\left(2\omega\nu_c-i\right)\mu_+\Gamma_+ +\mu_-\Gamma_-\left[\mu_+-2\omega\left(1+\rho_-\nu_c\right)\right]}{2\omega-2\omega\nu_c\sqrt{1+8\omega i}+i\rho_+}$$
$$-\frac{\nu_c\omega^2 K\left(\omega+i\rho_-/2\right)+\omega\left(1+\nu_c\rho_-\right)}{2\omega-2\omega\nu_c\sqrt{1+8\omega i}+i\rho_+},$$

$$K_{20} = \mu_+\Gamma_+,$$

$$L = 2-6\nu_c(1-\sigma)+6\nu_c^2(1-\sigma)^2,$$

$$L_{20} = \omega\nu_c\frac{2\left(\mu_+-\rho_+\right)\left(\mu_+\Gamma_+ +\mu_-\Gamma_-\right)-\omega K\left(\omega+i\rho_+/2\right)-\rho_+}{2\omega-2\omega\nu_c\sqrt{1+8\omega i}+i\rho_+}-\mu_+\Gamma_+,$$

$$M_{20} = \Gamma_-\left(\mu_-+1\right)^{-1},$$

$$N_{20} = \mu_-\left(\mu_-+1\right)^{-1}\Gamma_- -\mu_+\left(\mu_++1\right)^{-1}\Gamma_+ -1,$$

$$O_{20} = -1-\frac{1}{\nu_c}\left(\mu_++1\right)^{-1}\Gamma_+ -\frac{i\omega}{2}K,$$

$$P_{20} = \Gamma_+\left(\mu_++1\right)^{-1}.$$

REFERENCES

[1] A. Bayliss and B. Matkowsky, *Two routes to chaos in condensed phase combustion*, SIAM J. Appl. Math., 50 (1990), pp. 437–459.

[2] A. F. Belyaev and L. D. Komkova, *Dependence of burning velocity of thermites on pressure*, Zh. Fiz. Khim., 24 (1950), pp. 1302–1311.

[3] M. R. Booty, S. B. Margolis, and B. J. Matkowsky, *Interaction of pulsating and spinning waves in condensed phase combustion*, SIAM J. Appl. Math., 46 (1986), pp. 801–843.

[4] I. Brailovsky and G. Sivashinsky, *Chaotic dynamics in solid fuel combustion*, Phys. D, 65 (1993), pp. 191–198.

[5] P. Dimitriou, J. Puszinski, and V. Hlavacek, *On the dynamics of equations describing gasless combustion*, Combust. Sci. Tech., 68 (1989), pp. 101–111.

[6] M. Frankel, V. Roytburd, and G. Sivashinsky, *A sequence of period doublings and chaotic pulsations in a free boundary problem modeling thermal instabilities*, SIAM J. Appl. Math., 54 (1994), pp. 1101–1112.

[7] M. L. Frankel, V. Roytburd, and G. Sivashinsky, *Complex dynamics generated by a sharp interface model of self-propagating high-temperature synthesis*, Combust. Theory Modelling, 2 (1998), pp. 479–496.

[8] M. Garbey, H. G. Kaper, G. K. Leaf, and B. J. Matkowsky, *Quasi-periodic waves and the transfer of stability in condensed-phase surface combustion*, SIAM J. Appl. Math., 52 (1992), pp. 384–395.

[9] L. K. Gross, *Weakly nonlinear dynamics of interface propagation*, Stud. Appl. Math., 108 (2002), pp. 323–350.

[10] L. K. Gross and J. Yu, *Weakly nonlinear and numerical analyses of dynamics in a solid combustion model*, SIAM J. Appl. Math., 65 (2005), pp. 1708–1725.

[11] S. B. Margolis, *Transition to nonsteady deflagration in gasless combustion*, Progr. Energy Combust. Sci., 17 (1991), pp. 135–162.

[12] B. J. Matkowsky and G. I. Sivashinsky, *Propagation of a pulsating reaction front in solid fuel combustion*, SIAM J. Appl. Math., 35 (1978), pp. 465–478.

[13] A. G. Merzhanov, *SHS processes: Combustion theory and practice*, Arch. Combustionis, 1 (1981), pp. 23–48.

[14] A. G. Merzhanov, A. K. Filonenko, and I. P. Borovinskaya, *New phenomena in combustion of condensed systems*, Dokl. Akad. Nauk USSR, 208 (1973), pp. 892–894 (in Russian); Soviet Phys. Dokl., 208 (1973), pp. 122–125 (English translation).

[15] Z. A. Munir and U. Anselmi-Tamburini, *Self-propagating exothermic reactions: The synthesis of high-temperature materials by combustion*, Mat. Sci. Rep., 3 (1989), pp. 277–365.
[16] K. G. Shkadinsky, B. I. Khaikin, and A. G. Merzhanov, *Propagation of a pulsating exothermic reaction front in the condensed phase*, Combust. Expl. Shock Waves, 7 (1971), pp. 15–22.
[17] G. I. Sivashinsky, *The structure of Bunsen flames*, J. Chem. Phys., 62 (1975), pp. 638–643.
[18] A. Varma, A. S. Rogachev, A. S. Mukasyan, and S. Huang, *Combustion synthesis of advanced materials: Principles and applications*, Adv. Chem. Engrg., 24 (1998), pp. 79–226.
[19] J. Yu, L. K. Gross, and C. M. Danforth, *Complex dynamic behavior during transition in a solid combustion model*, Complexity, 14 (2009), pp. 9–14; also available online from http://onlinelibrary.wiley.com/journal/10.1002/(ISSN)1099-0526.